Ternary Chalcogenides BaM x Te 2 (M = Cu, Ag): Syntheses, Modulated Crystal Structures, Optical Properties, and Electronic Calculations

Subhendu Jana, Mohd Ishtiyak, Gopabandhu Panigrahi, Jai Prakash, Adel Mesbah, Saber Gueddida, Sébastien Lebègue, Christos Malliakas, James Ibers

Ternary Chalcogenides BaM_xTe_2 (M = Cu, Ag): Syntheses, Modulated Crystal Structures, Optical Properties, and Electronic Calculations

Subhendu Jana,[†] Mohd Ishtiyak,[†] Gopabandhu Panigrahi,[†] Jai Prakash,[†,‡] Adel Mesbah,[§,‡] Saber Gueddida,[⊥] Sébastien Lebègue,[⊥] Christos D. Malliakas,[‡] and James A. Ibers[‡,*]

[†]Department of Chemistry, Indian Institute of Technology Hyderabad, Kandi, Sangareddy, Telangana 502285, India

[‡]Department of Chemistry, Northwestern University, 2145 Sheridan Road, Evanston, IL 60208-3113, United States

[§] ICSM, Univ Montpellier, CEA, CNRS, ENSCM, Site de Marcoule, Bagnols-sur-Cèze, France

[⊥] Laboratoire de Physique et Chimie Théoriques (LPCT, UMR CNRS 7019), Institut Jean Barriol, Université de Lorraine, BP 239, Boulevard des Aiguillettes, Vandoeuvre-lès-Nancy 54506, France

ABSTRACT: Standard solid-state methods produced black crystals of the compounds $BaCu_{0.43(3)}Te_2$ and $BaAg_{0.77(1)}Te_2$ at 1173 K; the crystal structures of each were established using single-crystal X-ray diffraction data. Both crystal structures are modulated. The compound $BaCu_{0.43(3)}Te_2$ crystallizes in the monoclinic superspace group $P2(\alpha\beta1/2)0$ having cell dimensions a = 4.6406(5) Å, b = 4.6596(5) Å, c = 10.362(1) Å, Z = 2, and an incommensurate vector $q = 0.3498(6)b^* + 1/2c^*$. The compound $BaAg_{0.77(1)}Te_2$ crystallizes in the orthorhombic $P2_12_12(\alpha00)000$ superspace group with cell dimensions a = 4.6734(1) Å, b = 4.6468(1) Å, c = 11.1376(3) Å, Z = 2, and an incommensurate vector $q = 0.364(2)a^*$. The asymmetric unit of the $BaCu_{0.43(3)}Te_2$ structure comprises eight crystallographically independent sites; that for $BaAg_{0.77(1)}Te_2$ comprises four. In these two structures each of the M (= Cu, Ag) atoms is connected to four Te atoms to make two-dimensional layers of $[M_xTe_{4/4}]^{n-}$ that are separated by layers of Ba atoms and square nets of Te. A Raman spectroscopic study at 298(2) K on a pelletized polycrystalline sample of $BaAg_{0.8}Te_2$ shows the presence of Ag−Te (83, 116, and 139 cm^{-1}) and Ba−Te vibrations (667 $cm^{-1}$and 732cm^{-1}). A UV−vis-NIR spectroscopic study on a powdered sample of $BaAg_{0.8}Te_2$ shows the semiconducting nature of the compound with a direct band gap of 1.0(2) eV consistent with its black color. DFT calculations give a pseudo bandgap with a weak value of the DOS at the Fermi level.

INTRODUCTION

The structural chemistry of multinary metal chalcogenides [chalcogens (Q = S, Se, and Te)] is richer and more complex than that of the metal oxides because the chalcogens have lower electronegativity than Oxygen. This leads to less ionic character of metal-chalcogen bonds, increased covalent character, and less repulsion between the anions. The combination of these factors results in the formation of a variety of Q−Q bonding in the metal chalcogenides.[1–3]

The chalcogens can form various species starting from a simple Q_2^{2-} unit [e.g., $Ba_2Ag_2Se_2(Se_2)$,[4] $ZrTe_3$,[5] and Rb_2Te_2[6]] to complex nonlinear Q_n^{2-} units [e.g., Te_{13}^{2-} unit in Cs_2Te_{13}[7]], and hypervalent $(Q_n)^{m-}$ motifs (m, n > 2, Se_3^{4-} in $Ba_2Ag_4Se_5$,[8] Se_5^{4-} in Nb_2Se_9,[9] and Te_5^{4-} in NaTe[10]). Among the chalcogens, Te shows the most varied catenations. Te can form infinite chains (Ba_3ScTe_5,[11] $Gd_3Cu_2Te_7$,[12] and $LaCu_{0.40}Te_2$[13]), square nets ($EuCu_{0.66}Te_2$,[14] $Na_{0.2}Ag_{2.8}EuTe_4$,[14] KCu_2EuTe_4,[14] and $K_{0.33}Ba_{0.67}AgTe_2$[15]), and neutral Te_8 rings (e.g., Cs_4Te_{28})[7]. In most of these structures, the charge balance of the compounds can be achieved by the Zintl-Klemm concept.[16] However, charge-balancing in structures with infinite chalcogen chains and square nets is extremely difficult. Many of the initial reports of these structures showed equidistant Te atoms in these chains and square nets; theoretically these chains and nets are not stable and should be distorted. Hence, the crystal structures of many of these compounds (e.g. $LnTe_3$, and Ln_2Te_5)[17–21] upon reinvestigation displayed weak superstructure reflections indicating that the Te chains and nets are in fact distorted. These structural distortions are believed to be responsible for their intriguing physical properties such as charge density waves (CDW) in the $AMLnTe_4$ (A = K, Na; M = Cu, Ag; Ln = La, Ce) structures.[22,23] The average charges on these Te nets also vary depending on the structure type. For instance, the average charge on the Te atoms in the Te nets in quasi two-dimensional-structures of $LnTe_3$ compounds is $-0.5e^-$ whereas it decreases $-1e^-$ in the Ln_2Te_3 structures. Thus, the physical properties of these square-net chalcogenides show a strong correlation with the charge on their Te atoms and the nature of the interactions between neighboring Te atoms. These different types of Q–Q interactions can stabilize new unprecedented and unexpected structures that we seek to discover by exploratory syntheses.

In the last few decades, we have focused on the exploratory syntheses of ternary and quaternary new transition metal/actinide chalcogenides and have reported a number of

compounds that show a variety of new structure types with various chalcogen-chalcogen interactions. The flexibility of chalcogens to adopt various polyanionic units could not have been predicted have been but discovered depended on exploratory syntheses.

The chemistries of the actinides (An = Th, U, Np) are relatively unexplored. Consequently, actinide metal chalcogenides present an exciting area for exploratory chemistry. Generally such efforts fail; a few yield new compounds and surprising structures. Others yield new compounds that can only be prepared with the assistance of the actinides. Such is the case here where we present the syntheses, modulated crystal structures, Raman spectroscopy, optical properties, and electronic properties of two new compounds $BaCu_xTe_2$ and $BaAg_xTe_2$, which were discovered serendipitously while exploring the Ba−Th−Cu/Ag−Te systems. $BaCu_xTe_2$ could on be prepared with the assistance of Th.

EXPERIMENTAL METHODS

Syntheses and Analyses. *Caution*! *^{232}Th is an α-emitting radioisotope and as such is considered to be a health risk. Experiments using radioisotopes require appropriate infrastructure and personnel trained in the handling of radioactive materials.*

The following starting materials were used as supplied: Ba rod (Alfa Aesar, 99+ %), Ag flakes (Sigma Aldrich, 99.9%), Cu powder (Sigma Aldrich, 99.9%), Th powder (MP Biomedicals, 99.1%), and Te ingot (Sigma Aldrich, 99.999%). These chemicals were handled inside an Ar-filled glove box.

Synthesis of Single Crystals of $BaCu_xTe_2$. Black plate-shaped crystals of $BaCu_xTe_2$ were synthesized by standard solid-state methods. $BaCu_xTe_2$ crystals were first obtained serendipitously during an attempt to synthesize a new quaternary phase in the Ba−Th−Cu−Te system. First, Ba (35.5 mg, 0.259 mmol), Th (15 mg, 0.065 mmol), Cu (8.2 mg, 0.129 mmol), and Te (107.2 mg, 0.84 mmol) were loaded into a carbon-coated fused-silica tube (OD 6 mm) inside an Ar-filled glove box. The tube was then evacuated to *ca*. 10^{-4} Torr before being sealed. The tube was placed inside a programmable muffle furnace and heated to 1073 K in 36 h where it was kept for 15 h. The temperature of the furnace was then raised to 1173 K. The tube was kept for 198 h at 1173 K. Then it was cooled to 973 K in 96 h and then to 573 K in 100 h and then the furnace was turned off. The silica ampoule was opened under ambient condition and a

black lump was found. The lump was gently broken into small pieces before being examined under a microscope. The product contained black plate-shaped crystals. The energy-dispersive X-ray (EDS) spectroscopy analysis of these crystals was carried out with the help of a Hitachi S3400 scanning electron microscope. Semi-quantitative EDS analysis of the crystals showed the presence of Ba, Cu, and Te and no trace of Th. The compositions of these crystals were close to $BaCu_{0.7}Te_2$ (Ba:Cu:Te ≈ 1:0.70:2). Other phases found were black plates of ThOTe,[24] yellow BaTe,[25] and residual Te.

Synthesis of Single Crystals $BaAg_xTe_2$. Black plate-shaped crystals of a new ternary compound $BaAg_xTe_2$ were obtained during the exploration of Ba−Th−Ag−Te quaternary system in a reaction of Ba (23.67 mg, 0.172 mmol), Th (10 mg, 0.043 mmol), Ag (9.30 mg, 0.086 mmol), and Te (76.99 mg, 0.603 mmol). These reactants were first loaded into a carbon-coated fused-silica tube inside an Ar-filled glove box. The tube was flame sealed under vacuum (*ca.* 10^{-4} Torr) and then placed inside a computer-controlled muffle furnace. The heating profile of this reaction was the same as discussed above for the synthesis of $BaCu_xTe_2$ crystals. The reaction product of this reaction revealed the presence of black plates along with yellowish BaTe and unreacted Te. The EDS analysis of the plate-shaped crystals showed the presence of $BaAg_xTe_2$ (Ba:Ag:Te ≈ 1:0.8:2) along with ThOTe,[24] BaTe,[25] and Te crystals.

Syntheses of Polycrystalline $BaCu_xTe_2$ (x = 1.0, 0.85, 0.70, 0.55, and 0.43) and $BaAg_xTe_2$ (x = 1.0, 0.9, and 0.8) Attempts to synthesize polycrystalline samples of nominal compositions and $BaCu_xTe_2$ (x = 1.0, 0.85, 0.70, 0.55, and 0.43) and $BaAg_xTe_2$ (x = 1.0, 0.9, and 0.8) were carried out by the reactions of elemental Ba, Cu or Ag, and Te using the sealed tube solid-state synthesis method, as described earlier. These reactions were loaded with a total mass of 0.5-0.6 g. The sealed silica tubes were first heated to 823 K in 20 h from 298 K. After 24 h at 823 K, the temperature was ramped up to 973 K with a heating rate of 20 K/h. After 48 h the furnace was switched off, and the reactions were cooled to 298 K. The products were opened under ambient conditions. All these reactions produced homogenous black lumps or ingots. The lumps were then homogenized into fine powders inside an Ar-filled glove box. The powders of the loaded reactions were then individually compressed into 4 mm circular pellets by using 15 MPa pressure. Each of these pellets was again sealed inside a carbon-coated fused-silica tube. Each tube was heated to 773 K at 50 K/h. The temperature was kept constant at 773 K for 48 h.

Finally, the furnace was switched off. The resulting pellets were ground into homogeneous powders inside an Ar-filled glove box for further characterization. Powder X-ray diffraction (PXRD) patterns of these products were used to assess their phase purity.

Crystal Structure Determinations. Single crystal X-ray diffraction data for $BaCu_xTe_2$ were collected at 293(2) K on a STOE IPDS II diffractometer equipped with graphite monochromatized Mo radiation (λ = 0.71073Å) and an Image Plate (IP) detector. The data were collected with an ω-scan technique from 0º-180º at an arbitrary φ-angle. Data reduction was performed with the X-AREA package.[26] An analytical absorption correction was performed (*X*-SHAPE2 within X-AREA).[26]

Single crystal X-ray diffraction data from a $BaAg_xTe_2$ single crystal were collected at 100(2) K with the use of a Bruker APEX2 kappa diffractometer equipped with graphite-monochromatized Mo-$K\alpha$ radiation (λ = 0.71073 Å). The data collection strategy was optimized with the use of the algorithm COSMO in the APEX2 package as a series of ω and φ scans.[27] Scans of 0.5º at 60 s/frame were used. The detector-to-crystal distance was 60 mm. The collection of intensity data as well as cell refinement and data reduction were carried out with the use of the program APEX3.[27] An analytical absorption correction was performed using JANA2006.[28–30]

Both structures are modulated. Atomic coordinates of the atoms in the subcells and initial values of their modulation functions were determined by the charge-flipping method.[29,30] The incommensurate superstructures were refined with JANA2006 software.[28–30]

The subcell of the $BaCu_{0.43(3)}Te_2$ compound was indexed with an orthogonal cell a = 4.6406(5) Å, b = 4.6596(5) Å, c = 10.362(1) Å, and the satellite reflections (supercell) were located at a diagonal incommensurate vector q = 0.3499(6)b^*. None of the acceptable orthorhombic space groups gave a satisfactory refinement and structure was refined in the monoclinic superspace group $P2(\alpha\beta1/2)0$ (Table 1) with two Ba sites, two Cu sites, and four Te sites. Vacancies on the sites of Cu atoms were freely refined to the final stoichiometry $BaCu_{0.43(3)}Te_2$. Satellite reflections of one order were observed for $BaCu_{0.43(3)}Te_2$. Modulation waves of one order for positional and thermal displacement parameters were used for all Ba and Te atoms. There was no significant positional ordering of the Cu atoms; therefore, only the

modulation terms of the occupancy parameters were refined. An inversion twin law [-1 0 0 0 -1 0 0 0 -1] was considered with a refined value of 0.6 (40)%.

The subcell of the $BaAg_{0.77(1)}Te_2$ compound was indexed with an orthogonal cell a = 4.6734(1) Å, b = 4.6468(1) Å, c = 11.1376(3) Å, and the satellite reflections (supercell) were located at an incommensurate vector $q = 0.364(2)a^*$. The only orthorhombic space groups that gave good agreement indices for both the subcell and satellite reflections was $P2_12_12(\alpha 00)000$ (Table 1). There are total of four independent crystallographic sites, one Ba site, one Ag site, and two Te sites, in the asymmetric unit. Vacancies on the sites of Ag were freely refined to the final stoichiometry $BaAg_{0.77(1)}Te_2$. Satellite reflections of one order were observed for $BaAg_{0.77(1)}Te_2$. Modulation waves of one order for positional and thermal displacement parameters were used for all atoms. Only the symmetry allowed Fourier terms were refined. A twin law for racemic mixtures was used in the refinement. The electron density maps around the Cu2 atom of $BaCu_{0.43(3)}Te_2$ structure are shown in Supporting Information. The CRYSTALMAKER program was used to make all the drawings. Further details about the crystal structures are given in Table 1.

Table 1. Crystal Data and Structure Refinement for $BaCu_{0.43(3)}Te_2$ and $BaAg_{0.77(1)}Te_2$.

Empirical formula	$BaCu_{0.43(3)}Te_2$	$BaAg_{0.77(1)}Te_2$
Formula weight	420.1	476
Temperature (K)	293(2)	100(2)
Wavelength	0.71073 Å	0.71073 Å
Crystal system	monoclinic	orthorhombic
Space group	$P2(\alpha\beta1/2)0$	$P21212(\alpha00)000$
Unit cell dimensions	a = 4.6406(5) Å b = 4.6596(5) Å, β = 90.000(9)° c = 10.3620(15) Å	a = 4.67340(10) Å b = 4.64680(10) Å c = 11.1376(3) Å
q-vector(1)	$0a^* + 0.3499(6)b^* + 0.5c^*$	$0.364(2)a^*$
Volume	224.06(5) $Å^3$	241.868(10) $Å^3$
Z	2	2
Density (calculated)	6.23 g/cm^3	6.54 g/cm^3
Absorption coefficient	23.4 mm^{-1}	22.9 mm^{-1}
$F(000)$	345	393
Crystal size	0.372 × 0.301 × 0.014 mm^3	0.09 × 0.07 × 0.04 mm^3
θ range for data collection	4.75 to 38.15°	1.59 to 38.11°
Index ranges	-8<=h<=8, -8<=k<=8, -18<=l<=18, -1<=m<=1	-8<=h<=8, -8<=k<=7, -18<=l<=18, -1<=m<=1
Reflections collected	23635 (7798 main + 15837 satellites)	22714 (7558 main + 15156 satellites)
Independent reflections	2446 (2421 main + 4865 satellites) [R_{int} = 0.1052]	3757 (1257 main + 2500 satellites) [R_{int} = 0.1411]
Completeness to θ = 38.15°	99%	98%
Refinement method	Full-matrix least-squares on F^2	Full-matrix least-squares on F^2
Data / constrains / restraints / parameters	2446 / 5 / 0 / 87	3757 / 0 / 0 / 60
Goodness-of-fit on F^2	2.21	1.03
Final R indices [I>2σ(I)]	R_{obs} = 0.0679, wR_{obs} = 0.1091	R_{obs} = 0.0567, wR_{obs} = 0.0824
R indices [all data]	R_{all} = 0.1166, wR_{all} = 0.1187	R_{all} = 0.1989, wR_{all} = 0.1045
Final R main indices [I>2σ(I)]	R_{obs} = 0.0323, wR_{obs} = 0.0636	R_{obs} = 0.0440, wR_{obs} = 0.0726
R main indices (all data)	R_{all} = 0.0423, wR_{all} = 0.0652	R_{all} = 0.0776, wR_{all} = 0.0783
Final R 1st order satellites [I>2σ(I)]	R_{obs} = 0.1788, wR_{obs} = 0.2845	R_{obs} = 0.1626, wR_{obs} = 0.2648
R 1st order satellites (all data)	R_{all} = 0.2936, wR_{all} = 0.3158	R_{all} = 0.5469, wR_{all} = 0.4324
Extinction coefficient	12(15)	80(20)
Twin law [-1 0 0 0 -1 0 0 0 -	0.0(4)	0.5

1]		
T_{min} and T_{max} coefficients	0.3778 and 0.6923	0.2015 and 0.442
Largest diff. peak and hole	5.61 and -5.01 e·Å^{-3}	10.67 and -11.64 e·Å^{-3}

$R = \Sigma||F_o|-|F_c|| / \Sigma|F_o|$, $wR = \{\Sigma[w(|F_o|^2 - |F_c|^2)^2] / \Sigma[w(|F_o|^4)]\}^{1/2}$ and $w = 1/(\sigma^2(I)+0.0004I^2)$

Powder X-ray Diffraction (PXRD) Study. The phase purities of the polycrystalline samples of $BaCu_xTe_2$ and $BaAg_xTe_2$ were analyzed by PXRD studies at 298(2) K using an X'Pert Pro-PAN analytical diffractometer. A Cu-$K\alpha$ source of radiation (λ = 1.5406 Å) and an Xcelerator detector were used during the data collection. The operating current and voltage were 30 mA, and 40 kV, respectively. The reflection data were collected over a 2θ region of 10°−70° using a step size and scan time of 0.01° and 50 minutes, respectively. The simulated PXRD patterns were obtained from the single crystal data of BaM_xTe_2 using the deposited data and the Mercury program.[31]

Solid-State Ultraviolet (UV)-Visible (VIS) Near-Infrared (NIR) Spectroscopy. Optical absorption studies on powdered samples of $BaAg_{0.8}Te_2$ were carried at 298(2) K using a JASCO V-770 UV/VIS/NIR spectrophotometer in diffuse reflectance mode. Dried $BaSO_4$ powder was used as a standard reference. The reflectance data as a function of wavelength were recorded over a wavelength range from 2000 nm (0.62 eV) to 200 nm (6.2 eV). The reflectance data were converted to absorption data by using the Kubelka–Munk equation[32]:

$$\alpha/S = (1 - R)^2/2R \qquad (1)$$

Here α, R, and S are the absorption coefficient, the reflectance, and the scattering coefficient, respectively. The bandgap was estimated by using the Tauc plot[33]:

$$(\alpha h\upsilon)^n = A(h\upsilon - E_g) \qquad (2)$$

Here α, h, and υ are absorption coefficient, Planck's constant, and frequency of light, respectively. E_g is the bandgap and A is a proportionality constant. The value of constant n determines the nature of bandgap. n = 2 and n = ½ values signify direct and indirect band gap, respectively.

Raman Spectroscopy. The Raman spectra of pelletized polycrystalline $BaAg_{0.8}Te_2$ were collected at 298(2) K using a Bruker SENTERRA II dispersive micro Raman spectrometer

equipped with a confocal microscope. The spectra were recorded over a region of 50 to 3500 cm^{-1} with a resolution of 3.5 cm^{-1}. An excitation wavelength of 532 nm was used during the data collection. Raman spectra of individual pellets taken at different positions on the pellets showed no noticeable changes.

Electronic Structure Calculations. Because we cannot treat partial occupancies, we have considered the formulas $BaCuTe_2$ and $BaAgTe_2$ in order to obtain a qualitative understanding of the electronic structure of the compounds studied experimentally. The first principles calculations were carried out with the Vienna Ab Initio Simulation Package (VASP)[34] code using the projector augmented wave method.[35,36] For the exchange-correlation functional, we adopted the generalized gradient approximation with the Perdew, Burke, and Ernzerhof parametrization[37–39] to relax the crystal structure and then the Heyd, Scuseria, and Ernzerhof functional to compute the density of states (DOS).[40,41] The integration over the Brillouin zone was sampled by 6 × 6 × 2 k-points for the two compounds. The kinetic energy cutoff for the expansion of the wave functions was set to the default value for both compounds.

RESULTS AND DISCUSSION

Syntheses. While exploring the Ba−Th−M−Te (M = Cu/Ag) system, we discovered black plate-shaped single crystals of $BaCu_xTe_2$ and $BaAg_xTe_2$ in the reactions of the elements at 1173 K. The yields of these two phases were around 30% based on M. The Th-free reaction for the $BaAg_xTe_2$ phase using the same reaction conditions did produce the desired $BaAg_xTe_2$ phase but the quality of the crystals was poor. In contrast, the $BaCu_xTe_2$ crystals could not be reproduced using the Th-free reaction of Ba, Cu, and Te. The crystals of BaM_xTe_2 were stable in air for at least one week. To study the stability of these phases, the syntheses of polycrystalline samples of $BaCu_xTe_2$ (x = 1.0, 0.85, 0.70, 0.55, and 0.43) and $BaAg_xTe_2$ (x = 1.0, 0.9, and 0.8) were attempted by reactions of the elements using a two-step sealed tube method. The PXRD patterns of the final products of the $BaCu_xTe_2$ (x = 1.0 and 0.43) and $BaAg_xTe_2$ (x = 1.0, 0.9, and 0.8) reactions are shown in Figure 1. The PXRD patterns of $BaCu_xTe_2$ (x = 0.85, 0.70, and 0.55) are shown in the Supplementary Information.

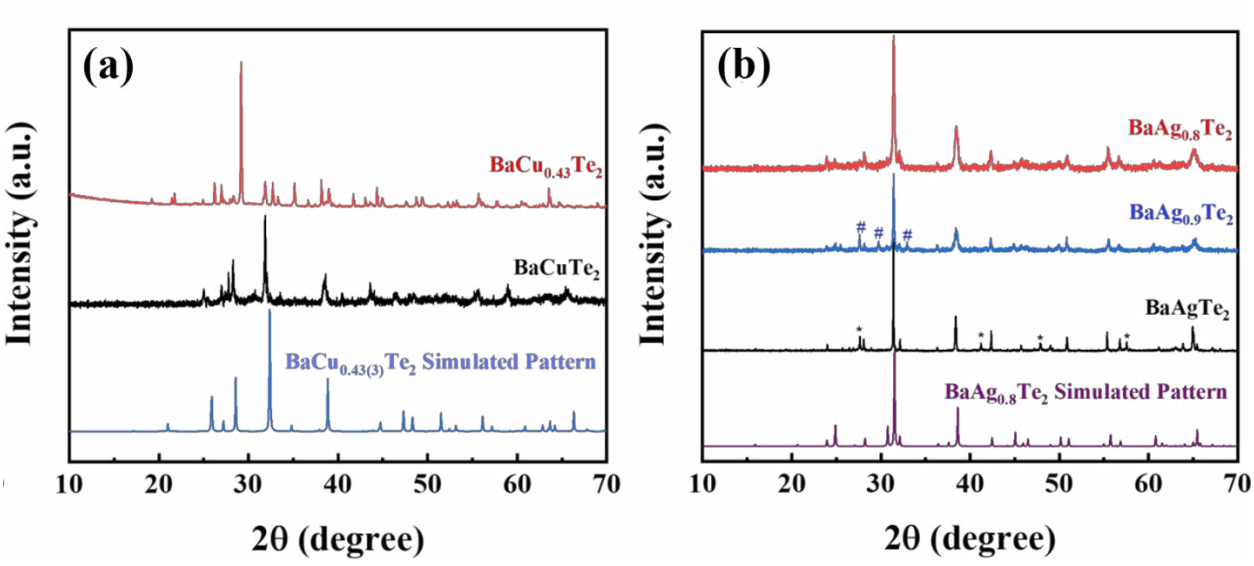

Figure 1: Powder X-ray diffraction patterns of **(a)** $BaCu_xTe_2$ (x = 1.0 and 0.43) along with the simulated PXRD pattern of $BaCu_{0.43(3)}Te_2$ structure and **(b)** $BaAg_xTe_2$ (x = 0, 0.9, and 0.8). The unindexed reflections for PXRD patterns of $BaAgTe_2$ and $BaAg_{0.9}Te_2$ phases are shown by * and # symbols, respectively. The PXRD pattern of loaded composition $BaCu_{0.43}Te_2$ completely matches with a known phase $Ba_{6.76}Cu_{2.42}Te_{14}$ ($BaCu_{0.37}Te_{2.07}$).[42]

The PXRD pattern of the loaded composition $BaCu_{0.43}Te_2$ shows the formation of monophasic $Ba_{6.76}Cu_{2.42}Te_{14}$[42] instead of the target $BaCu_xTe_2$ phase. The products of the $BaCu_xTe_2$ (x = 0.85, 0.70, 0.55) reactions also show the presence of the known ternary phase, $Ba_{6.76}Cu_{2.42}Te_{14}$ ($BaCu_{0.37}Te_{2.07}$)[42] as a major phase along with small amounts of BaTe (See S. I.). Interestingly, the PXRD pattern for x = 1.0 composition did not show the presence of the known $Ba_{6.76}Cu_{2.42}Te_{14}$ phase, but also could not be indexed completely based on the $BaCu_{0.43(3)}Te_2$ pattern simulated from the single-crystal X-ray structure determination. These observations suggest that $BaCu_{0.43(3)}Te_2$ is a kinetically stabilized phase that can only be synthesized by the Th-assisted reaction. No further attempts were made to synthesize $BaCu_{0.43(3)}Te_2$ phase by modifying the elemental ratios or heating profiles of Th-free reactions.

For $BaAg_xTe_2$ (x = 1.0, 0.9, and 0.8), most reflections matched the PXRD pattern calculated from the single-crystal data of $BaAg_{0.77(1)}Te_2$, but there were some unindexed reflections observed for the x = 1.0 and 0.9 phases. These unindexed reflections did not match known phases, including barium tellurides, silver tellurides, and $BaAg_2Te_2$ nor did we detect the presence of any unreacted reactants (Ba, Ag, and Te) in the PXRD patterns. The phase purity of x = 0.8 sample i.e. $BaAg_{0.8}Te_2$ is very close to the composition ($BaAg_{0.77(1)}Te_2$) obtained from the single crystal data (Figure 1). Hence, this polycrystalline sample with a loaded composition of $BaAg_{0.8}Te_2$, was used for further characterization and physical property measurements.

Crystal Structures of BaM_xTe_2 (M = Cu, Ag).

The superstructure of the $BaCu_{0.43(3)}Te_2$ compound was solved in the monoclinic superspace group $P2(\alpha\beta1/2)0$ with cell constants of a = 4.6406(5) Å, b = 4.6596(5) Å, c = 10.362(1) Å, and a incommensurate vector $q = 0.3499(6)b^* + 1/2c^*$. The superstructure contains two Ba sites, two Cu sites, and four Te sites. The refinement of vacancies at the sites of Cu and the Te(1) atoms lead to the final stoichiometry of $BaCu_{0.43(3)}Te_2$. The average atomic distances for $BaCu_{0.43(3)}Te_2$ are given in Table 2 and the average subcell structure is shown in Figure 2(a).

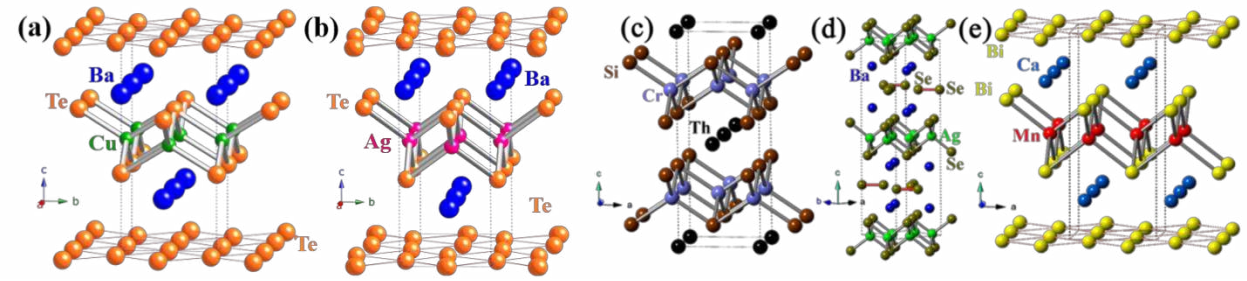

Figure 2: Average subcell structures of unit cells of **(a)** $BaCu_{0.43(3)}Te_2$ and **(b)** $BaAg_{0.77(1)}Te_2$, and views of the unit cells of **(c)** $ThCr_2Si_2$, **(d)** $BaAgSe_2$, and **(e)** $CaMnBi_2$ structures.

Table 2. Average Interatomic Distances (in Å) in the Superstructure of BaM_xTe_2 (M = Cu, Ag).

	M = Cu, x = 0.43(3)			M = Ag, x = 0.77(1)		
	Average	Minimum	Maximum	Average	Minimum	Maximum
M1−Te1	-	-	-	2.865(2) × 2 2.879(3) × 2	2.854(3) × 2 2.863(4) × 2	2.877(3) × 2 2.895(4) × 2
M1−Te3	2.73(2) × 2	2.71(2) × 2	2.75(2) × 2	-	-	-
M1−Te4	2.72(2) × 2	2.70(2) × 2	2.74(2) × 2	-	-	-
M2−Te3	2.74(2) × 2	2.72(2) × 2	2.75(2) × 2	-	-	-
M2−Te4	2.72(2) × 2	2.70(2) × 2	2.74(2) × 2	-	-	-
Te1···Te2	3.293(5) × 1 3.294(5) × 1 3.298(5) × 1 3.297(5) × 1	3.002(7) × 2 2.996(7) × 2	3.604(7) × 2 3.608(7) × 2	-	-	-
Te2···Te2	-	-	-	3.299(2) × 2 3.302(2) × 1 3.304(2) × 1	3.028(3) × 4	3.584(3) × 4
Ba1−Te1	3.58(2) × 1 3.59(2) × 1	3.46(2) × 2	3.72(2) × 2	3.500(2) × 4	3.461(2) × 2 3.467(2) × 2	3.540(2) × 2 3.534(2) × 2
Ba1−Te2	3.61(2) × 2	3.58(2) × 2	3.64(2) × 2	3.563(2) × 2	3.444(4) × 2	3.684(4) × 2

Ba1−Te3	3.44(1) × 4	3.41(1) × 2 3.38(1) × 2	3.46(1) × 2 3.49(1) × 2	-	-	-
Ba2−Te1	3.65(2) × 2	3.61(2) × 2	3.68(2) × 2			
Ba2−Te2	3.62(2) × 2	3.50(2) × 2	3.74(2) × 2	-	-	-
Ba2−Te4	3.43(1) × 4	3.37(1) × 2 3.41(1) × 2	3.49(1) × 2 3.46(1) × 2	-	-	-

In the superstructure of $BaCu_{0.43(3)}Te_2$ each of the Cu atoms is coordinated to four Te atoms (two Te3 and two Te4), forming a distorted $CuTe_4$ tetrahedral unit. The $CuTe_4$ tetrahedra are fused by the sharing of all edges. This results in the formation of infinite two-dimensional layers of $[Cu_{0.43(3)}Te_{4/4}]^{1.57-}$. These layers of $[Cu_{0.43(3)}Te_{4/4}]^{1.57-}$ are extended along the *bc* plane. The arrangement of Cu and Te atoms in these layers can be classified as the anti-PbO type.[43,44] These $[Cu_{0.43(3)}Te_{4/4}]^{1.57-}$ layers are further separated by the layer of Ba1 and Ba2 atoms followed by a tellurium square net that is made up of Te1 and Te2 atoms (Figure 2a). In the superstructure of $BaCu_{0.43(3)}Te_2$, the average Cu1−Te and Cu2−Te distances are 2.72(2) Å−2.73(2) Å and 2.72(2) Å−2.74(2) Å, respectively. These distances are consistent with the Cu−Te distances in the related structures such as $Cu_{0.66}EuTe_2$ (2.671(4) Å),[14] $LaCu_{0.40}Te_2$ (2.611(3) Å−2.781(4) Å),[13] $KCuCeTe_4$ (2.667(4) Å),[22] and $NaCuZrTe_3$ (2.619(7) Å−2.695(7) Å).[45]

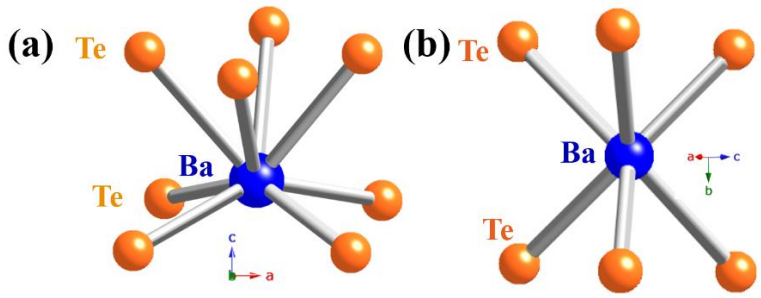

Figure 3: Coordination environments of Ba atoms in the **(a)** $BaCu_{0.43(3)}Te_2$ and **(b)** $BaAg_{0.77(1)}Te_2$ substructures, respectively.

Each of the Ba atoms in the superstructure of $BaCu_{0.43(3)}Te_2$ is connected to a total of eight Te atoms in a square antiprism geometry (Figure 3a). The average Ba1−Te and Ba2−Te distances (3.43(1) Å to 3.65(2) Å) are comparable with the Ba−Te distances in $K_{0.33}Ba_{0.67}AgTe_2$ (3.526(3) Å and 3.596(3) Å),[15] $BaAgTbTe_3$ (3.431(1) Å−3.822(1) Å),[46] and $BaAgYTe_3$ (3.434(1) Å−3.812(1) Å).[47]

The average distances between Te1 and Te2 atoms in the square nets of Te atoms range from 3.293(5) Å to 3.298(5) Å. These distances are shorter than the van der Waals interactions of ~4.0 Å between two Te atoms and longer than a Te−Te single bond distance (~2.8 Å). A comparison of Te···Te interactions with related known compounds is presented in Table 3.

As discussed above, our attempts to synthesize polycrystalline $BaCu_xTe_2$ ($x<1$) led to formation of the known $Ba_{6.76}Cu_{2.42}Te_{14}$ (or $BaCu_{0.37}Te_{2.07}$) compound as the major phase. The The compound crystallizes in space group $P6_3/mcm$ of the hexagonal system (see Figure S3 in S.I.). Its three-dimensional structure is composed of Ba cations that fill the channels made by $CuTe_4$ tetrahedral units and bent Te_3^{2-} units. Unlike $BaCu_{0.43(3)}Te_2$ structure, $Ba_{6.76}Cu_{2.42}Te_{14}$ contains conventional Te−Te bonding in the Te_3^{2-} units, and hence charge balance for this compound is achieved as $(Ba^{2+})_{6.76}(Cu^{+})_{2.42}(Te_3^{2-})_3(Te^{2-})_5$.

Table 3. Intermediate Te···Te Interactions in Some Related Layered Structures.

Compound	Te···Te distance (Å)	Ref
$BaCu_{0.43(3)}Te_2$	3.29(1)	This work
$BaAg_{0.77(1)}Te_2$	3.30(1)	This work
$EuCu_{0.66}Te_2$	3.168(1)	14
KCu_2EuTe_4	3.1371(4)	14
$K_{0.33}Ba_{0.67}Te_2$	3.269(2)	15
$LaTe_2$	3.187(2)	19
$Na_{0.2}Ag_{2.8}EuTe_4$	3.1497(3)	14

The superstructure of $BaAg_{0.77(1)}Te_2$ was also found to be incommensurate, but different from that of $BaCu_{0.43(3)}Te_2$. It was solved in the orthorhombic $P2_12_12(\alpha 00)000$ superspace group with cell dimensions of a = 4.6734(1) Å, b = 4.6468(1) Å, c = 11.1376(3) Å, and an incommensurate vector $q = 0.364(2)a^*$. The asymmetric unit of the structure comprises a total of four independent crystallographic sites, one Ba, one Ag, and two Te sites.

The composition of this compound freely refined to the final stoichiometry $BaAg_{0.77(1)}Te_2$. The average atomic distances for $BaAg_{0.77(1)}Te_2$ are tabulated in Table 2. A view of the unit cell of the average subcell structure of $BaAg_{0.77(1)}Te_2$ is shown in Figure 2b. Each Ag atom in this structure is bonded to four Te1 atoms in a slightly distorted tetrahedral geometry similar to the Cu-coordination in the $BaCu_{0.43(3)}Te_2$ structure. These $AgTe_4$ tetrahedra are fused together by sharing of all edges to form infinite two-dimensional layers of $[Ag_{0.77(1)}Te_{4/4}]^{1.23-}$. The coordination number of Ba atoms in this structure is six and the geometry is trigonal prismatic (Figure 3b) in contrast to square-antiprismatic geometry of Ba in the $BaCu_{0.43(3)}Te_2$ structure.

The average Ag1−Te1 distances of 2.865(2) Å to 2.879(3) Å in $BaAg_{0.77(1)}Te_2$ are in good agreement with the Ag^{1+}−Te distances in $BaAg_2Te_2$ (2.775(7) Å−2.938(8) Å),[48] $K_{0.33}Ba_{0.67}AgTe_2$ (2.905(2) Å),[15] and $Na_{0.2}Ag_{2.8}EuTe_4$ (2.829(6) Å−2.949(7) Å).[14] The average Ba−Te distances are in the range of 3.500(2) Å to 3.563(2) Å. The average distance between two neighboring Te2 atoms is 3.30(2) Å which is very close to the average Te···Te interactions of 3.293(5) Å−3.298(5) Å in the $BaCu_{0.43(3)}Te_2$ structure.

Both the $BaCu_{0.43(3)}Te_2$ and $BaAg_{0.77(1)}Te_2$ structures show modulation of theirTe square nets. The minimum, maximum, and average Te···Te interactions in $BaAg_{0.77(1)}Te_2$ are 3.03(1) Å, 3.58(1) Å, and 3.30(1) Å, which are significantly different from each other. This long-range modulation of Te square nets is akin to those compounds that show charge density wave (CDW) waves.[49–51] There are also modulations in the Ag−Te and Ba−Te distances (Table 2). These modulations in the Te square nets, Ag−Te distances, and Ba−Te distances contribute to the overall distortion in the $BaAg_{0.77(1)}Te_2$ structure. The modulation of $BaCu_{0.43(3)}Te_2$ structure is also mainly attributed to the modulation in the Te···Te interactions in the Te square nets, Cu−Te distances in $[M_xTe_{4/4}]^{n-}$ layers, and Ba−Te distances in $BaTe_8$ square antiprism. The average,

shortest, and maximum Te···Te interactions, Cu−Te, and Ba−Te distances are tabulated in Table 2.

Structural Relationships Among $ThCr_2Si_2$,[52] $BaAgSe_2$,[4] BaM_xTe_2, and $CaMnBi_2$.[53] The substructures of BaM_xTe_2 are related to the well-known structures of $ThCr_2Si_2$, $BaAgSe_2$, and $CaMnBi_2$. The unit cell structures of $ThCr_2Si_2$, $BaAgSe_2$, and $CaMnBi_2$ are shown in Figure 2. All the compounds but $ThCr_2Si_2$ have predominantly two-dimensional crystal structures. The Th atoms of $ThCr_2Si_2$ structure have bonding interactions with Si atoms.[54] A common feature of these structure types is the presence of tetrahedral layers of transition-metal with chalcogen/pnictogen/tetrel. The compositions of these layers are $[Cr_2Si_2]^{4-}$, $[AgSe_{4/4}]^{1-}$, $[M_xTe_{4/4}]^{n-}$, and $[MnBi_{4/4}]^{1-}$. The arrangement of atoms in these layers is of the anti-PbO type.[43,44] The main difference among these structures is the composition of the chemical species that separate their layers and the number of layers per unit cell. The tetragonal $ThCr_2Si_2$ structure (space group $I4/mmm$) and monoclinic $BaAgSe_2$ structure (space group $P2_1/c$) contain two layers per unit cell whereas the BaM_xTe_2 and $CaMnBi_2$ structures contain only one layer per unit cell (Figure 2). The $[M_xTe_{4/4}]^{n-}$ layers in the BaM_xTe_2 structure are separated by Ba cations and distorted square planes of Te atoms in contrast to the $BaAgSe_2$ structure where Ba cations and Se_2^{2-} dimers separate the $[AgSe_{4/4}]^{1-}$ layers. The $[Cr_2Si_2]^{4-}$ layers in $ThCr_2Si_2$ are separated only by Th atoms. Both BaM_xTe_2 and $BaAgSe_2$ can be considered as 122-type compounds if one ignores the M-vacancy, but still these structures are very different. The more pronounced catenation tendency Te > Se may be the reason for the stabilization of the BaM_xTe_2 structure with distorted Te squares instead of the monoclinic $BaAgSe_2$ type structure.

Assignment of Formal Oxidation States. As discussed earlier, the $BaAg_{0.77(1)}Te_2$ substructure consists of three layers ($[Ag_{0.77(1)}Te1]$, Ba1, and Te2 square net). Here, the oxidation states of Ag1, Ba1, and Te1 may be assigned as +1, +2, and −2, respectively. However, the assignment of an oxidation state for the Te2 atom involved in the formation of square nets is difficult and arbitrary owing to intermediate Te−Te interactions and silver deficiency. It is well established that the arrangement of Te in a perfect square net or linear chains with distances close to 2.8 Å (single Te−Te bond distance) will lead to Peierls distortion as these nets according

to theoretical considerations are unstable.[55,56] These square nets can get stabilized if the charge on each Te is −2 (i.e., 8 electrons in the valence shell of the Te atom), which requires non-bonding interactions among neighboring Te atoms. If the effective charge on the Te atom is less negative then −2) it will lead to the stabilization of homoatomic bonding interactions between Te−Te atoms and the formation of polytelluride oligomers.[56] Electronic band structure calculations for a hypothetical ideal square net of Te atoms with oxidation state less negative then −2 should give a metal-like band structure where the Fermi energy (E_F) levels crosses one or more bands.[15] But actually the distorted square nets of Te atoms with extended Te−Te interactions leads to the opening of a band gap, and semiconducting properties. Such distortion results in the formation of strong and weak Te−Te interactions where the effective charge on each Te atom in the distorted Te square nets depends on the extent of modulation/distortion, which is also controlled by the overall charge on the $[M_xTe]^{n-}$ layers. Indeed, $BaAg_xTe_2$ single crystal data show satellite reflections indicative of a distorted modulated superstructure.

If one assumes the full occupancy of the transition-metal site, then the chemical formula will be $BaMTe_2$ with layers of $[M^{1+}Te^{2-}]^{1-}$. Then the charged-balanced formula can be written as $[(Ba^{2+})(M^{+}Te^{2-})(Te^{1-})]$. The transition-metal deficiency in our compounds should lower the average oxidation state of Te2 atoms of the square net to less than −1. This implies that the occupancy of M atom is equal to the negative charge on the Te2 atoms. This corresponds to −0.8 e^- charge when the Ag occupancy is 80% i.e., $[(Ba^{2+})(Ag^{0.8+}Te^{2-})(Te^{0.8-})]$. The structure of $BaAg_{0.77(1)}Te_2$ is similar to that of $K_{0.33}Ba_{0.67}AgTe_2$ (space group: *I*4/*mmm*).[15] The main difference in these two structures is a vacancy at the Ag site of the two-dimensional layer in $BaAg_{0.77(1)}Te_2$ whereas in $K_{0.33}Ba_{0.67}AgTe_2$[15] the Ba and K cations that separate the two-dimensional layers of [AgTe] are disordered at one crystallographic site. This leads to a formal charge of −0.67 for each of the Te atoms in the Te square net. The structure of $BaCu_{0.43(3)}Te_2$ has a vacancy at the transition metal site, is similar to the vacancy of Cu atoms in the two dimensional $[Cu_xTe_{4/4}]^{n-}$ layer in $EuCu_{0.66}Te_2$ (space group: *P*4/*mmm*). In $EuCu_{0.66}Te_2$, the effective charge on each Te atom in the square net is −0.66. This type of vacancy in the transition metal site is common in antimonides having the formula of M_xLaSb_2 (M = Zn, Cu, and Mn; x = 0.52 – 0.87).[57]

Optical Bandgap of $BaAg_{0.8}Te_2$.

An absorption spectrum of a homogeneously ground polycrystalline sample of $BaAg_{0.8}Te_2$ was collected at 298(2) K over a wavelength region of 2000 nm to 200 nm.

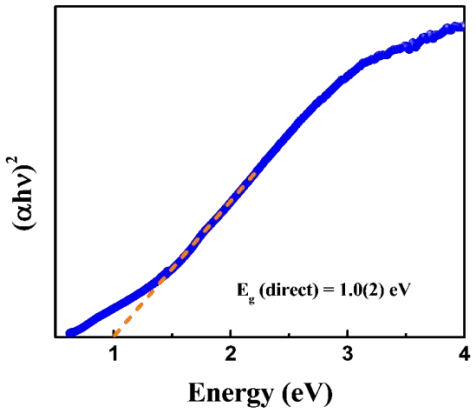

Figure 4: Tauc plot of solid-state UV-Vis-NIR spectrum of powdered polycrystalline $BaAg_{0.8}Te_2$.

The absorption edge study shows that $BaAg_{0.8}Te_2$ is a narrow band gap semiconductor with a direct bandgap of 1.0(2) eV, which agrees with the black color of the compound. The indirect bandgap of this compound is below 0.62 eV, which is beyond the limit of the instrument used in this study. Hence, the only direct bandgap is shown in Figure 4.

Raman Spectroscopy. A Raman spectrum of a pelletized polycrystalline sample of $BaAg_{0.8}Te_2$ was recorded at 298(2) K. The most intense bands around 83 cm^{-1}, 116 cm^{-1}, and 139 cm^{-1} (Figure 5) are Ag−Te stretching modes. These bands can be compared with the Ag−Te stretching modes of 80 cm^{-1}, 110 cm^{-1}, and 138 cm^{-1} in Ag_2Te.[58] The bands at 667 $cm^{-1}$and 732 cm^{-1} are Ba−Te stretching modes, in good agreement with the Ba−Te stretching frequencies in $BaIn_2Te_4$ (667 cm^{-1} and 732 cm^{-1})[33] and Ba_3ScTe_5 (671.5 cm^{-1} and 730 cm^{-1}).[11]

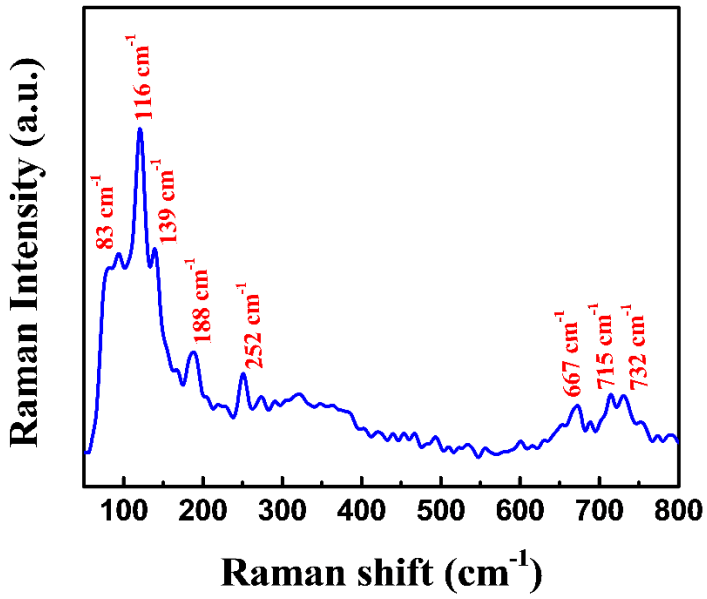

Figure 5: Raman spectrum of a powdered polycrystalline $BaAg_{0.8}Te_2$ sample.

Electronic Structure Calculations. Figure 6 shows our calculated total (upper panel) and partial (lower panels) density of states (DOS) for $BaCuTe_2$ and $BaAgTe_2$. Our calculations show that the two systems are metals, although the total DOS presents a relatively small value at the Fermi level and give a weak metallic character to the system. This is mainly because of the contributions of the p-orbitals of the Te atoms (see the partial DOS), whereas the contributions from Ba atoms (d-orbitals) are almost negligible. Also, the Ag and Cu atoms do not contribute to the DOS around the Fermi level.

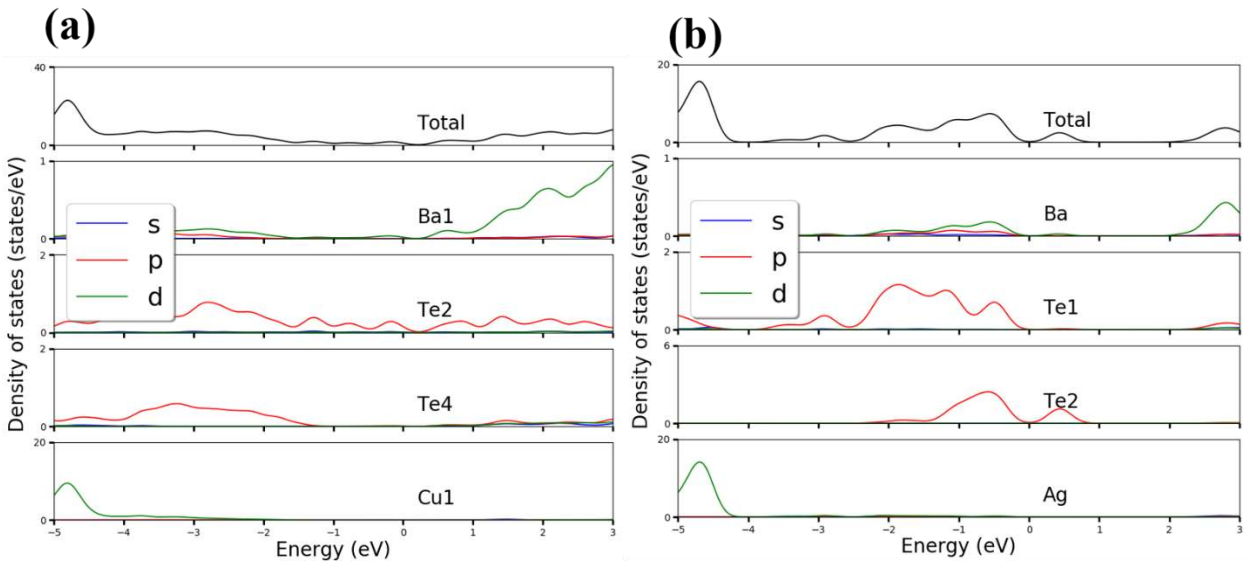

Figure 6: The calculated total (upper panel) and partial (lower panels) density of states (DOS) for **(a)** $BaCuTe_2$ and **(b)** $BaAgTe_2$.

CONCLUSIONS

Single crystals of two new ternary tellurides, BaM_xTe_2 (M = Cu, Ag) have been synthesized at 1173 K using solid-state synthesis methods. Single crystal X-ray diffraction studies show that both structures are modulated. $BaCu_{0.43(3)}Te_2$ crystallizes in the incommensurate monoclinic superspace group $P2(\alpha\beta1/2)0$ with the cell constants of a = 4.6406(5) Å, b = 4.6596(5) Å, c = 10.362(1) Å and an incommensurate vector $q = 0.3499(6)b^* + 1/2c^*$ (Z = 2). There are eight crystallographically unique positions (two Ba, two Cu, four Te). The compound $BaAg_{0.77(1)}Te_2$ crystallizes in the orthorhombic incommensurate superspace group $P2_12_12(\alpha00)000$ having cell lengths of a = 4.6734(1) Å, b = 4.6468(1) Å, c = 11.1376(3) Å, and an incommensurate $q = 0.364(2)a^*$ (Z = 2). The asymmetric unit of $BaAg_{0.77(1)}Te_2$ unit cell contains four crystallographically independent positions (one Ba, one Ag, two Te). Each of the M atoms are connected to four Te atoms making a tetrahedral unit that share edges to make two-dimensional layers of $[M_xTe_{4/4}]^{n-}$. Ba atoms and distorted Te square nets separate these layers. A Raman spectroscopic study at 298(2) K on a pelletized polycrystalline sample of $BaAg_{0.8}Te_2$ shows the presence of Ag−Te (83, 116, and 139 cm^{-1}) and Ba−Te vibrations (667 $cm^{-1}$and 732 cm^{-1}). A UV−vis-NIR spectroscopic study shows the compound to be a semiconductor with a

direct band gap of 1.0(2) eV, consistent with its black color. DFT calculations give a pseudo bandgap with a weak value of the DOS at the Fermi level.

AUTHOR INFORMATION

Corresponding Author

*E-mail: ibers@chem.northwestern.edu

ORCID

James A. Ibers: 0000-0002-5418-3645

Notes The authors declare no competing financial interest.

SUPPORTING INFORMATION

CCDC #1998322 and 1998323 contain supplementary crystallographic data for the superstructures. These data may be obtained free of charge by emailing data_request@ccdc.ccam.ac or www.ccdc.cam.ac.uk/data_request/cif or by contacting the Crystallographic Data Centre. 12 Union Road, Cambridge CB2 1EZ, UK; fax +44 1223 336033. For the superstructure CCDC is unable to handle modulated structures but the raw fcf data are included with this submission. Supporting information includes details on reaction conditions, additional PXRD plots, atomic coordinates, interatomic distances and angles, and displacive details for $BaCu_{0.43(3)}Te_2$ and $BaAg_{0.77(1)}Te_2$ substructures.

ACKNOWLEDGMENTS

J.P. thanks the Science and Engineering Research Board (SERB), Department of Science and Technology (DST), Government of India, for financial support under an Early Career Research award (Grant ECR/2017/000822) and IIT Hyderabad for seed grant and research facilities. S. J. and G. P. thank Ministry of Human Research Development and IIT Hyderabad for research fellowships. M.I. thanks DST India for research fellowship. Use was made of the Integrated Molecular Structure Education and Research Center X-ray Facility at Northwestern University, which has received support from the Soft and Hybrid Nanotechnology Experimental Resource

(NSF Grant ECCS-1542205), the State of Illinois, and the International Institute for Nanotechnology.

References:

(1) Cody, J. A.; Mansuetto, M. F.; Pell, M. A.; Chien, S.; Ibers, J. A. New one-dimensional ternary and quaternary cesium-metal-tellurium compounds. *J. of Alloys Compd.* **1995**, *219*, 59–62.

(2) Mar, A.; Jobic, S.; Ibers, J. A. Metal-Metal vs Tellurium-Tellurium Bonding in WTe_2 and Its Ternary Variants $TaIrTe_4$ and $NbIrTe_4$. *J. Am. Chem. Soc.* **1992**, *114*, 8963–8971.

(3) Rouxel, J. Low-Dimensional Solids: An Interface between Molecular and Solid-State Chemistry? The Example of Chainlike Niobium and Tantalum Chalcogenides. *Acc. Chem. Res.* **1992**, *25*, 328–336.

(4) Jana, S.; Ishtiyak, M.; Mesbah, A.; Lebègue, S.; Prakash, J.; Malliakas, C. D.; Ibers, J. A. Synthesis and Characterization of $Ba_2Ag_2Se_2(Se_2)$. *Inorg. Chem.* **2019**, *58*, 7837–7844.

(5) Stöwe, K.; Wagner, F. R. Crystal Structure and Calculated Electronic Band Structure of $ZrTe_3$. *J. Solid State Chem.* **1998**, *138*, 160–168.

(6) Böttcher, P.; Getzschmann, J.; Keller, R. Zur Kenntnis der Dialkalimetalldichalkogenide β-Na_2S_2, K_2S_2, α-Rb_2S_2, β-Rb_2S_2, K_2Se_2, Rb_2Se_2, α-K_2Te_2, β-K_2Te_2 und Rb_2Te_2. *Z. Anorg. Allg. Chem.* **1993**, *619*, 476–488.

(7) Sheldrick, W. S.; Wachhold, M. Synthesis and structure of Cs_2Te_{13} and Cs_4Te_{28}, tellurium-rich tellurides on the methanolothermal route to Cs_3Te_{22}. *Chem. Commun.* **1996**, 607–608.

(8) Assoud, A.; Xu, J.; Kleinke, H. Structures and Physical Properties of New Semiconducting Polyselenides $Ba_2Cu_\delta Ag_{4-\delta}Se_5$ with Unprecedented Linear Se_3^{4-} Units. *Inorg. Chem.* **2007**, *46*, 9906–9911.

(9) Meerschaut, A.; Guémas, L.; Berger, R.; Rouxel, J. The crystal structure of niobium selenide Nb_2Se_9 from twin-crystal data, *Acta Cryst.* **1979**, *B35*, 1747–1750.

(10) Böttcher, P.; Keller, R. The Crystal Structure of NaTe and Its Relationship to Tellurium-Rich Tellurides. *J. Less Common Met.* **1985**, *109*, 311–321.

(11) Ishtiyak, M.; Panigrahi, G.; Jana, S.; Prakash, J.; Mesbah, A.; Malliakas, C. D.; Lebègue, S.; Ibers, J. A. Modulated Linear Tellurium Chains in Ba_3ScTe_5: Synthesis, Crystal Structure, Optical and Resistivity Studies, and Electronic Structure. *Inorg. Chem.* **2020**, *59*, 2434–2442.

(12) Huang, F. Q.; Ibers, J. A. $Gd_3Cu_2Te_7$ and $U_2Cu_{0.78}Te_6$: Two Examples of Linear Te

Chains. *J. Solid State Chem.* **2001**, *159*, 186–190.

(13) Huang, F. Q.; Brazis, P.; Kannewurf, C. R.; Ibers, J. A. Syntheses, Structures, Physical Properties, and Theoretical Study of $LaCu_{0.40}Te_2$, $NdCu_{0.37}Te_2$, $SmCu_{0.34}Te_2$, $GdCu_{0.33}Te_2$, and $DyCu_{0.32}Te_2$. *J. Am. Chem. Soc.* **2000**, *122*, 80–86.

(14) Patschke, R.; Brazis, P.; Kannewurf, C. R.; Kanatzidis, M. G. $Cu_{0.66}EuTe_2$, KCu_2EuTe_4 and $Na_{0.2}Ag_{2.8}EuTe_4$: compounds with modulated square Te nets. *J. Mater. Chem.* **1999**, *9*, 2293–2296.

(15) Zhang, X.; Li, J.; Foran, B.; Lee, S.; Guo, H.-Y.; Hogan, T.; Kannewurf, C. R.; Kanatzidis, M. G. Distorted Square Nets of Tellurium in the Novel Quaternary Polytelluride $K_{0.33}Ba_{0.67}AgTe_2$. *J. Am. Chem. Soc.* **1995**, *117*, 10513–10520.

(16) Nesper, R. The Zintl-Klemm Concept - A Historical Survey. *Z. anorg. allg. Chem.* **2014**, *640*, 2639–2648.

(17) Norling, B. K.; Steinfink, H. The Crystal Structure of Neodymium Tritelluride. *Inorg. Chem.* **1966**, *5*, 1488–1491.

(18) Ramsey, T. H.; Steinfink, H.; Weiss, E. J. The Phase Equilibria and Crystal Chemistry of the Rare Earth-Group VI Systems. IV. Lanthanum-Tellurium. *Inorg. Chem.* **1965**, *4*, 1154–1157.

(19) Wang, R.; Steinfink, H.; Bradley, W. F. The Crystal Structure of Lanthanum Telluride and Tellurium-Deficient Neodymium Telluride. *Inorg. Chem.* **1966**, *5*, 142–145.

(20) Lin, W.; Steinfink, H.; Weiss, E. J. The Phase Equilibria and Crystal Chemistry of the Rare Earth Group VI Systems. III. Neodymium-Tellurium. *Inorg. Chem.* **1965**, *4*, 877–881.

(21) Muravieva, V. K.; Pomelova, T. A.; Tarasenko, M. S.; Kuratieva, N. V.; Naumov, N. G. Crystal Structure of $LnTe_3$, Where Ln = La, Ho. *J. Struct. Chem.* **2017**, *58*, 1676–1680.

(22) Patschke, R.; Heising, J.; Kanatzidis, M.; Brazis, P.; Kannewurf, C. R. $KCuCeTe_4$: A New Intergrowth Rare Earth Telluride with an Incommensurate Superstructure Associated with a Distorted Square Net of Tellurium. *Chem. Mater.* **1998**, *10*, 695–697.

(23) Patschke, R.; Kanatzidis, M. G. Polytelluride compounds containing distorted nets of tellurium. *Phys. Chem. Chem. Phys.* **2002**, *4*, 3266–3281.

(24) Beck, H. P.; Dausch, W. Die Verfeinerung der Kristallstruktur von ThOTe. *Z. Anorg. Allg.*

Chem. **1989**, *571*, 162–164.

(25) Wyckoff, R. W. G. *Crystal Structures*, 2nd ed.; Interscience Publishers: New York, 1963; Vol. *1*.

(26) *X-SHAPE; Stoe & Cie: Darmstadt, Germany, 2002*.

(27) *Bruker APEX2 Version 2009.5-1 Data Collection and Processing Software; Bruker Analytical X-Ray Instruments, Inc.: Madison, WI*, 2009.

(28) Petříček, V.; Dušek, M.; Palatinus, L. Crystallographic Computing System JANA2006: General Features. *Zeitschrift Für Kristallogr. - Cryst. Mater.* **2014**, *229*, 345–352.

(29) Oszlányi, G.; Sütő, A. *Ab initio* structure solution by charge flipping. II. use of weak reflections. *Acta Cryst.* **2005**, *A61*, 147–152.

(30) Oszlányi, G.; Sütő, A. *Ab initio* structure solution by charge flipping. *Acta Cryst.* **2004**, *A60*, 134–141.

(31) Macrae, C. F.; Sovago, I.; Cottrell, S. J.; Galek, P. T. A.; McCabe, P.; Pidcock, E.; Platings, M.; Shields, G. P.; Stevens, J. S.; Towler, M.; Wood, P. A. *Mercury 4.0* : from visualization to analysis, design and prediction. *J Appl Crystallogr* **2020**, *53*, 226–235.

(32) Kortüm, G. *Reflectance Spectroscopy: Principles, Methods, Applications*; Springer-Verlag: New York, 1969.

(33) Ishtiyak, M.; Jana, S.; Narayanswamy, S.; Nishad, A. K.; Panigrahi, G.; Bhattacharjee, P. P.; Prakash, J. Intrinsic extremely low thermal conductivity in $BaIn_2Te_4$: Synthesis, crystal structure, raman spectroscopy, optical, and thermoelectric properties. *J. Alloys Compd.* **2019**, *802*, 385–393.

(34) Kresse, G.; Joubert, D. From ultrasoft pseudopotentials to the projector augmented-wave method. *Phys. Rev.* **1999**, *59*, B1758–B1775.

(35) Blöchl, P. E. Projector Augmented-wave method. *Phys. Rev. B* **1994**, *50*, 17953–17979.

(36) Perdew, J. P.; Burke, K.; Ernzerhof, M. Generalized Gradient Approximation Made Simple. *Phys. Rev. Lett.* **1996**, *77*, 3865–3868.

(37) Heyd, J.; Scuseria, G. E.; Ernzerhof, M. Hybrid functionals based on a screened coulomb potential. *J. Chem. Phys.* **2003**, *118*, 8207–8215.

(38) Heyd, J.; Scuseria, G. E.; Ernzerhof, M. Erratum: “Hybrid functionals based on a screened coulomb potential” [J. Chem. Phys. 118, 8207 (2003)]. *J. Chem. Phys.* **2006**, *124*, 219906.

(39) Paier, J.; Marsman, M.; Hummer, K.; Kresse, G.; Gerber, I. C.; Ángyán, J. G. Screened hybrid density functionals applied to solids. *J. Chem. Phys.* **2006**, *124*, 154709.

(40) Kohn, W.; Sham, L. J. Self-consistent equations including exchange and correlation effects. *Phys. Rev.* **1965**, *140*, A1133–A1138.

(41) Hohenberg, P.; Kohn, W. Inhomogeneous Electron Gas. *Phys. Rev.* **1964**, *136*, B864–B871.

(42) Cui, Y.; Assoud, A.; Xu, J.; Kleinke, H. Structures and Physical Properties of New Semiconducting Gold and Copper Polytellurides: $Ba_7Au_2Te_{14}$ and $Ba_{6.76}Cu_{2.42}Te_{14}$. *Inorg. Chem.* **2007**, *46*, 1215–1221.

(43) Margadonna, S.; Takabayashi, Y.; McDonald, M. T.; Kasperkiewicz, K.; Mizuguchi, Y.; Takano, Y.; Fitch, A. N.; Suard, E.; Prassides, K. Crystal structure of the new $FeSe_{1-x}$ superconductor. *Chem. Commun.* **2008**, 5607–5609.

(44) Guo, J.; Jin, S.; Wang, G.; Wang, S.; Zhu, K.; Zhou, T.; He, M.; Chen, X. Superconductivity in the iron selenide $K_xFe_2Se_2$ ($0 \leq x \leq 1.0$). *Phys. Rev. B* **2010**, *82*, 180520.

(45) Mansuetto, M. F.; Keane, P. M.; Ibers, J. A. Synthesis and Structures of the New Group IV Chalcogenides $NaCuTiS_3$ and $NaCuZrQ_3$ (Q = S, Se, Te). *J. Solid State Chem.* **1993**, *105*, 580–587.

(46) Prakash, J.; Mesbah, A.; Beard, J. C.; Ibers, J. A. Syntheses and Crystal Structures of $BaAgTbS_3$, $BaCuGdTe_3$, $BaCuTbTe_3$, $BaAgTbTe_3$, and $CsAgUTe_3$. *Z. Anorg. Allg. Chem.* **2015**, *641*, 1253–1257.

(47) Yang, Y.; Ibers, J. A. Synthesis and Characterization of a Series of Quaternary Chalcogenides Ba*LnMQ*$_3$ (*Ln* = Rare Earth, *M* = Coinage Metal, *Q* = Se or Te). *J. Solid State Chem.* **1999**, *147*, 366–371.

(48) Assoud, A.; Cui, Y.; Thomas, S.; Sutherland, B.; Kleinke, H. Structure and physical properties of the new telluride $BaAg_2Te_2$ and its quaternary variants $BaCu_\delta Ag_{2-\delta}Te_2$. *J. Solid State Chem.* **2008**, *181*, 2024–2030.

(49) Malliakas, C. D.; Kanatzidis, M. G. A Double Charge Density Wave in the Single Tellurium Square Net in $Cu_{0.63}EuTe_2$? *J. Am. Chem. Soc.* **2009**, *131*, 6896–6897.

(50) Malliakas, C.; Billinge, S. J. L.; Kim, H. J.; Kanatzidis, M. G. Square Nets of Tellurium:

Rare-Earth Dependent Variation in the Charge-Density Wave of $RETe_3$ (RE = Rare-Earth Element). *J. Am. Chem. Soc.* **2005**, *127*, 6510–6511.

(51) Kim, H. J.; Malliakas, C. D.; Tomić, A. T.; Tessmer, S. H.; Kanatzidis, M. G.; Billinge, S. J. L. Local Atomic Structure and Discommensurations in the Charge Density Wave of $CeTe_3$. *Phys. Rev. Lett.* **2006**, *96*, 226401.

(52) Ban, Z.; Sikirica, M. The Crystal Structure of Ternary Silicides ThM_2Si_2 (M = Cr, Mn, Fe, Co, Ni and Cu). *Acta. Cryst.* **1965**, *18*, 594–599.

(53) Brechtel, E.; Cordier, G.; Schäfer, H. Zur Darstellung und Struktur von $CaMnBi_2$, *Z. Naturforsch. B* **1980**, *35*, 1–3.

(54) Shatruk, M. $ThCr_2Si_2$ structure type: The "perovskite" of intermetallics. *J. Solid State Chem*. **2019**, *272*, 198–209.

(55) Peierls, R. *More Surprises in Theoretical Physics*; Princeton University Press: Princeton, NJ, 1991.

(56) Papoian, G. A.; Hoffmann, R. Hypervalent Bonding in One, Two, and Three Dimensions: Extending the Zintl–Klemm Concept to Nonclassical Electron-Rich Networks. *Angew. Chem. Int. Ed.* **2000**, *39*, 2408–2448.

(57) Cordier, G.; Schäfer, H.; Woll, P. Besetzungsvarianten der $CaMnBi_2$- Struktur: Zur Kenntnis der Verbindungen $LaZn_{0.52}Sb_2$, $LaCo_{0.68}Sb_2$, $LaMn_xSb_2$ ($0.65 \leq x \leq 0.76$) und $LaCu_xSb_2$ ($0.82 \leq x \leq 0.87$). *Z. Naturforsch.* **1985**, *40b*, 1097–1099.

(58) Milenov, T. I.; Tenev, T.; Miloushev, I.; Avdeev, G. V.; Luo, C. W.; Chou, W. C. Preliminary studies of the Raman spectra of Ag_2Te and Ag_5Te_3. *Opt. Quant. Electron.* **2014**, *46*, 573–580.